Journal of Environmental Chemical Engineering 8 (2020) 103981

Contents lists available at ScienceDirect

Journal of Environmental Chemical Engineering

journal homepage: www.elsevier.com/locate/jece

Amino-functionalised silica-grafted molecularly imprinted polymers for chloramphenicol adsorption

Z. Mohamed Idris[a,b,c], B.H. Hameed[d], L. Ye[c], S. Hajizadeh[c], B. Mattiasson[e], A.T. Mohd Din[a,*]

[a] School of Chemical Engineering, Engineering Campus, Universiti Sains Malaysia, 14300, Nibong Tebal, Penang, Malaysia
[b] Department of Chemical Engineering Technology, Faculty of Engineering Technology, Universiti Malaysia Perlis, Kampus UniCITI Alam, Sg. Chuchuh, 02100, Padang Besar, Perlis, Malaysia
[c] Division of Pure and Applied Biochemistry, Lund University, Box 124, 221 00, Lund, Sweden
[d] Department of Chemical Engineering, College of Engineering, Qatar University, P.O. Box 2713, Doha, Qatar
[e] Division of Biotechnology, Lund University, Box 124, 221 00, Lund, Sweden

ARTICLE INFO

Editor: Despo Kassinos

Keywords:
Molecularly imprinted polymer
Precipitation polymerisation
Adsorption
Chloramphenicol
Emerging contaminant

ABSTRACT

This research investigated the liquid-phase removal of chloramphenicol (CAP), an emerging contaminant using molecularly imprinted polymers (MIPs). CAP adsorption profiles, equilibrium, and kinetics were analysed. The adsorption performance was compared between MIPs and non-imprinted polymers (NIPs), both with silica or without silica grafting. The imprinting factor (IF) values for the Si@MIPs-CAP were significantly higher than the IF values for MIPs-CAP adsorbent at pH 8. The kinetics of CAP adsorption was fitted to pseudo-second-order kinetics models for MIPs-CAP (R^2 = 0.9998) and Si@MIPs-CAP (R^2 = 0.9999). The adsorption isotherm of Si@MIPs-CAP was well represented by the Langmuir model (R^2 = 0.9991), while the Freundlich isotherm model (R^2 = 0.9998) provided the best fit for MIPs-CAP. The maximum monolayer adsorption capacities, Q_{max}, for Si@MIPs-CAP (32.26 mg g^{-1}) were higher than the Q_{max} for Si@NIPs-CAP (29.6 mg g^{-1}). These results suggested that the silica-grafted molecularly imprinted polymers can be employed as a potential water-compatible adsorbent for the selective adsorption and removal of CAP from aqueous phase.

1. Introduction

Pharmaceuticals and personal care products (PPCPs) have been used since the end of the 19th century. However, the awareness of their persistence in the environment has only recently risen over the past few years, and considered as emerging contaminants (ECs) with potential hazards to the environment and human health [1]. Among the numerous PPCPs, antibiotics have become a major concern because they are extensively and increasingly used in human and veterinary drugs, resulting in their continuous release to the environment [2]. By 2030, the production of antibiotics is expected to increase up to 67%, especially in developing countries [1]. Chloramphenicol (CAP) is a synthetic antibiotic used for the treatment of bacterial infection in animals and for disease prevention [3]. However, the use of this antibiotic has been prohibited in many countries, such as the United States of America, Canada, China, and members of the European Union due to its adverse effect on human health (EFSA CONTAM Panel; 2014 [3],). It is associated with potentially serious side effects on human, such as gray baby syndrome, leukemia, fatal aplastic anaemia, and other blood disorders [4].

In Malaysia, CAP is still being illegally used based on the veterinary drug residues monitoring report conducted by the Department of Veterinary Services from 2010 to 2016 [5]. CAP is listed as a prohibited drug for food in Malaysia along with nitrofuran and beta agonists ([6], 2017). The continuous illegal usage of CAP is capable of contaminating animal food products and drinking water once this antibiotic penetrates the water stream. There is also a growing concern over the development of antimicrobial resistance towards chloramphenicol. Several isolated *E. coli* strains from aquaculture and environmental water samples in Sarawak, Malaysia were found to contain chloramphenicol resistance genes [7]. This result shows that prolonged exposure in the environment has made these microorganisms insusceptible to the antibiotic, which made the existing diseases difficult to treat. Thus, a comprehensive water treatment is required to separate and recover this antibiotic from the contaminated sources.

Molecular imprinting technology provides an alternative way to prepare adsorbent with high specificity and binding affinity towards target molecules. This technology is widely used for separation

* Corresponding author.
E-mail address: chazam@usm.my (A.T. Mohd Din).

https://doi.org/10.1016/j.jece.2020.103981
Received 9 December 2019; Received in revised form 15 April 2020; Accepted 20 April 2020
Available online 16 May 2020

purposes in chromatography, solid-phase extraction, microextraction, and adsorption of pollutants [8,9]. Molecularly imprinted polymers (MIPs) offer several advantages, such as mechanical and chemical stability, low cost, ease of preparation, and reversible adsorption and desorption ([10]; Ye, 2015). However, the adsorbent prepared using this method had poor molecular recognition in aqueous medium [11]. Developed MIPs are compatibly preferred by organic solvents and show higher non-specific binding due to its hydrophobic effect, which limits their application in an aqueous environment [12]. Numerous methods have been developed to produce water-compatible MIPs. Core-shell molecular imprinting method offers an alternative approach to prepare water-compatible adsorbents. This can be done by coating a hydrophilic layer onto the MIP shell, either using surface post-modification or grafting methods [13,14]. Usually, cores are synthesised as supporting materials for the MIPs shell and to ease the separation of the polymer particles after use. Therefore, modification on the surface of the core is a promising strategy to develop materials that would be water-compatible with MIPs, while offering several advantages, such as having higher surface area, improved polarity, decreased surface energy, and increased dispersibility and stability [15].

In this study, the silica core-shell of the molecularly imprinted polymers (Si@MIPs-CAP) were prepared by coating the MIPs onto the surface of amino-functionalised silica (Si@NH_2) nanoparticles. Silica was used in this study because it has an abundance of active hydroxyl groups that are necessary for surface modification. Modifying the silica core using vinyl groups is a traditional approach to enhance the adsorption and selectivity of silica MIPs. However, the use of organosilanes as surface modifiers is preferred because the flexibility of these modifiers, with respect to terminal functionalities, allows better control over the hydrophobicity or hydrophilicity of the surfaces. Silane coupling agents, such as γ-methacryloxypropyltrimethoxysilane (MPS), (3-aminopropyl)triethoxysilane (APTES), vinyltriethoxysilane (VTES), and (3-mercaptopropyl)trimethoxysilane (MPTMS) are the common organosilanes used for surface modification [13,16]. These silane coupling agents can form conjugation with the active hydroxyl groups on the surface of the silica core upon hydrolysis. The vinyl, amino, and thiol groups at the end of the silane molecule can improve the activity of silica and facilitate further modification of the organic functional groups. All these features have contributed to excellent adsorption capacity, high selectivity, and faster binding kinetics in the core-shell nanoparticles coated with molecularly imprinted polymers. Zhao et al. [17] has reported a successful application of vinyl-functionalized silica core using MPS to synthesize molecularly imprinted silica monolith for selective extraction of alpha-cypermethrin from soil samples. While, Mehdinia et al. [18] immobilized APTES onto the surface of magnetic silica core (Fe_3O_4@SiO_2) prior to copolymerization of MIPs shell, using 4-nitrophenol as the imprinted template. Also, MPTMS has been widely used to prepare thiol-functionalised silica support in ion-imprinting technique for removal of heavy metals [16]. In this work, a comparison study between MIPs-CAP and Si@MIPs-CAP was conducted to evaluate the effect of amino-functionalised silica nanoparticles on material characteristics and adsorption behaviours of the imprinted polymers. Adsorption kinetics and isotherms, as well as the effects of different solvents and different pH were also investigated.

2. Materials and methods

2.1. Materials

Tetraethylorthosilicate (TEOS), (3-Aminopropyl)triethoxysilane (APTES), triethylamine (TEA), chloramphenicol (CAP), ethylene glycol dimethacrylate (EDGMA, 98%), methacrylic acid (MAA, 99%), and ammonia were sourced from Sigma-Aldrich and used without further purification. 2,2′-Azobis(2-methylpropionitrile) (AIBN, 98%) was purchased from Merck (Darmstadt, Germany) and was recrystallised from methanol prior to use. Other chemicals (acetonitrile, ethanol, methanol, toluene, and acetone) were of analytical grade and were used as received. All solutions were prepared using ultrapure water (18.2 MΩ cm).

2.2. Preparation of silica particles

A one-pot synthesis of silica nanoparticles using the Stöber method was applied [19]. First, 100 mL of methanol, 33 mL of water, and 22.4 mL of 25% of ammonia were added into 1000 mL glass beaker, and agitated using a magnetic stirrer. A mixture of 30 mL of methanol and 13.8 mL of TEOS was quickly added to the solution. Then, the reaction mixture was stirred for 8 h at ambient temperature. The resulting silica particles were recovered via centrifugation at 4000 rpm. The particles were then washed three times with water, followed by methanol, before being placed in a vacuum desiccator to dry.

2.3. Preparation of amino-functionalised silica particles

The silica nanoparticles were immersed in 1% of APTES solution in 50 mL of anhydrous toluene. The solution was allowed to react at reflux temperature (110 °C), with constant stirring for 24 h. The particles were then washed with acetone and ethanol several times to remove residual reagents. They were then left to dry in a vacuum desiccator. The amino-functionalised silica particles were denoted as Si@NH_2 [19].

2.4. Preparation of polymer particles

The CAP-imprinted polymer particles were synthesised via precipitation polymerisation in acetonitrile [20]. The synthesis conditions are tabulated in the following Table 1. Briefly, the template (CAP) and the functional monomer (MAA) were dissolved in a round bottom flask (100 mL) using acetonitrile. Next, the cross-linker (EDGMA) and the initiator (AIBN) were added into the solution, and the solution mixture was sonicated for 5 min. Then, the solution mixture was purged with nitrogen for 5 min and the flask was sealed. Polymerisation was initiated at 60 °C with agitation and continued for 24 h. Following polymerisation, the solid particles were collected via centrifugation at 10,000 rpm for 10 min and washed twice with methanol. To remove the template, the solid particles were washed with a mixture of methanol/acetic acid (9:1, v/v) until no template was detected in the washing solvent. Finally, the solid particles were washed with acetone and dried in a vacuum desiccator. The obtained solid particles were denoted as MIPs-CAP. To prepare the silica core-shell imprinted polymer (denoted as Si@MIPs-CAP), the prepared Si@NH_2 particles were dispersed in the solution prior to the addition of EDGMA and AIBN. For comparisons,

Table 1
Synthesis conditions for preparation of imprinted polymer particles.

Polymer	CAP (mmol)	MAA (mmol)	EDGMA (mmol)	AIBN (mg)	Acetonitrile (mL)	Si@NH_2 (mg)
MIPs-CAP	0.25	1.0	2.4	28	15	–
NIPs-CAP	–	1.0	2.4	28	15	–
Si@MIPs-CAP	0.25	1.0	2.4	28	15	500
Si@NIPs-CAP	–	1.0	2.4	28	15	500

the non-imprinted polymers, namely, NIPs-CAP and Si@NIPs-CAP were synthesised similarly to MIPs-CAP and Si@MIPs-CAP, respectively, minus the addition of the template in the initial monomer solutions.

2.5. Characterisation of polymer particles

Attenuated total reflection (ATR) infrared spectra was recorded at room temperature in the range of 4000 to 525 cm^{-1}, with a resolution of 4 cm^{-1} and 16 scans using a Thermo-Fisher FT-IR instrument (Nicolet iS5, Thermo-Fisher Scientific Inc., Waltham, MA, USA). A scanning electron microscope (Thermal Field Emission SEM LEO 1560, Zeiss, Oberkochen, Germany) and a transmission electron microscope (Tecnai Spirit BioTWIN, FEI Company, Oregon, USA) were used to observe the surface morphologies of the particles. The surface area properties were obtained using a surface characterisation analyser (Micromeritics 3Flex, Micromeritics Instruments Corp., USA), with a bath temperature of 77 K.

2.6. Rebinding analysis

All rebinding experiments were conducted on a rocking table, while gently stirred at 298 K. In this study, two parameters (solvent and solution pH) that affect the binding capacities of the as-synthesised polymer particles (MIPs-CAP, Si@MIPs-CAP, NIPs-CAP, and Si@NIPs-CAP) were studied. To investigate the effect of different solvents on the adsorption of CAP, 5 mg of polymer particles were mixed with 100 mg L^{-1} of CAP in 1 mL of solvent (acetonitrile, water or solvent mixture). After 24 h, the particles were removed via centrifugation at 10,000 rpm for 10 min. Next, 50 µL of supernatant from each sample was collected, in which the concentration of CAP was determined using a UV/Vis spectrophotometer (Cary 60, Agilent Technologies, USA). The UV detection wavelength was set at 278 nm [21]. To evaluate the effect of different solution pH on the binding property of polymer particles, the same procedure for the solvent was followed, but the pH values were varied from 2 to 9. The experimental data are presented as the adsorption capacity per unit mass (g) of the polymer particles, and the adsorption capacity (Q_t) was calculated using the following Eq. (1):

$$Q_t = \frac{(C_0 - C_t)V}{W} \quad (1)$$

Where C_0 is the CAP initial concentration (mg L^{-1}), C_t is the CAP concentration at contact time, t (mg L^{-1}), V (mL) is the volume of the solution, and W (mg) is the mass of the polymer particles.

2.7. Batch adsorption studies

The batch equilibrium studies were performed at different initial concentrations of CAP (50–400 mg L^{-1}) in 1 mL of water (pH 7). The solutions were gently mixed with 5 mg of polymer particles on a rocking table at 298 K for 24 h to reach equilibrium. After incubation, the particles were sedimented via centrifugation and 50 µL of the supernatant from each sample was withdrawn, in which the concentration of CAP was determined using a UV/Vis spectrophotometer. All experimental data are presented as the adsorption capacity per unit mass (g) of the polymer particles, and the adsorption capacity at the respective contact time (Q_t) was calculated using Eq. (1). The adsorption capacity of the polymer particles at equilibrium (Q_e) was determined using the following Eq. (2):

$$Q_e = \frac{(C_0 - C_e)V}{W} \quad (2)$$

For the batch kinetics studies, the experiments were conducted at different contact times (20, 40, 80, 120, 180, 240, and 300 min) at room temperature. A volume of 1 mL CAP solution at known concentration of 100 mg L^{-1} (pH 7) was gently mixed with 5 mg of polymer particles on a rocking table. After incubation at preset time intervals (t), the particles were sedimented via centrifugation at 10,000 rpm for 10 min. Then, 50 µL of supernatant from each sample was withdrawn, in which the concentration of CAP was determined using a UV/Vis spectrophotometer.

2.8. Adsorption kinetics & isotherms

Adsorption kinetics models are important tools to determine the kinetics parameters and to predict the adsorption rate for designing and modelling the adsorption process. In this study, the kinetics of CAP adsorption on the different polymer particles were analysed using four different kinetics models, namely, pseudo-first order, pseudo-second order, Elovich, and Weber–Morris intra-particle diffusion models [22–24]. Experimental data fittings on Langmuir, Freundlich, Temkin, and Dubinin–Radushkevich adsorption isotherm models were performed to investigate the sorption mechanism, as well as the surface property and affinity of the polymer particles [25–28]. Expressions and details description of the abovementioned kinetics and adsorption isotherm models are provided in Appendices S1 and S2, respectively.

The conformity between the experimental data and the model predicted values was expressed by the linear correlation coefficient (R^2). A relatively high R^2 value (close or equal to 1) was used to indicate the best fit to the kinetics models. In addition, the applicability of each model for the respective adsorption system is further examined by calculating the sum-of-square-error (*SSE*) as presented by the following Eq. (3):

$$\mathrm{SSE} = \sqrt{\frac{\sum (Q_{e,exp} - Q_{e,cal})^2}{N}} \quad (3)$$

Where $Q_{e,exp}$ (mg g^{-1}) is the CAP adsorption capacity at equilibrium obtained from the experiment, $Q_{e,cal}$ (mg g^{-1}) is the CAP adsorption capacity at equilibrium calculated from the model, and N is the number of data points.

3. Results and discussion

3.1. Preparation of polymer particles

The CAP, an amide compound containing several reactive groups that can form hydrogen bonds. These groups are a para-nitro (p-NO_2) group, two hydroxyl (−OH) groups, an amine (-NH) group, and a carbonyl (C═O) group. CAP containing the amine group (-NH) is basic with pK_a of 8.69 (MarvinSketch 18.22, ChemAxon, 2018). Thus, an acid-base interaction can be formed between CAP and an acidic functional monomer. The MAA (pK_a 4.66) provides the carboxyl group (−COOH), which could strongly interact with the reactive groups on the CAP to form molecular recognition sites. The MAA is used extensively due to its ability to act as both hydrogen bond donor and hydrogen bond acceptor. The structures of the CAP, MAA, and CAP-MAA complex, as sketched using the MarvinSketch software (MarvinSketch 18.22, ChemAxon, 2018), are supplied in Fig. S1. EDGMA and acetonitrile were used as the cross-linker and solvent, respectively. EDGMA is commonly employed because it provides high cross-link ratios with sufficient mechanical stability.

Solvents also play an important role in the molecular imprinting process by functioning as the porogen (pore creator). While selecting a porogen, one must consider its role in promoting the template-functional monomer complex formation. The presence of hydroxyl (−OH) and amine (–NH) functional groups in a protic solvent can disturb the hydrogen bonds between the template and the functional monomer, thus reducing the formation of molecular recognition sites on the imprinted material. Therefore, an aprotic solvent can be used to increase the formation of the prepolymer complexes. Common solvents, such as acetonitrile, toluene, and chloroform have been used to prepare imprinted polymers. However, acetonitrile was employed in this study

because it has the highest dielectric constant (36.64) compared to chloroform (4.81) and toluene (2.38), which favoured the formation of the strongest hydrogen bonds between the template and the monomer. The application of a porogen solvent with a high dielectric constant has significantly improved the binding properties of imprinted polymers compared to corresponding non-imprinted polymers [29].

In this study, all polymer particles were prepared using precipitation polymerisation to obtain nanosphere particles. The temperature and the reaction time were fixed at 60 °C and 24 h, respectively, with CAP to MAA ratio of 1:4. It is recommended that the functional monomer be in excess relative to the number of moles of the template to favour the formation of template-monomer assemblies. However, if the amount of functional monomer is too high, non-specific interactions can occur [29]. Different template to monomer ratios can lead to a number of different configurations of the template-functional monomer complex, which could produce a heterogeneous binding site distribution. This could affect the molecular recognition ability of the imprinted polymer particles. The CAP:EDGMA ratio was selected at 1:10 in this study. The cross-linker could also have a significant impact on the physical characteristics of the imprinted polymer. However, it is less effective on the specific interactions between the template and the functional monomers. In the case of achieving polymerisation via the precipitation method, optimising the amount of the cross-linker and reducing the template concentration have improved the polymer binding properties and decreased the level of non-specific interactions [20]. Moreover, a high cross-linking degree would favour the formation of the most effective imprinting sites, leading to the highest imprinting factor and specific binding properties [30]. However, the amount of the cross-linker should be optimised and must be flexible enough to accommodate mass transfer inside the pores, while preserving the rigidity of the polymer.

Other parameters that were considered for molecularly imprinted polymer design were type and amount of initiator. AIBN was selected as the initiator because it would produce one type of free radicals with less side reaction and stable properties. In this study, the amount of AIBN used was 28 mg. These values were selected based on the results reported by Ren et al. [31]. Additional amount of the initiator (> 30 mg) was found to be less significant on the adsorption capacity of the molecularly imprinted polymers. If the initiator concentration is too high, it would disrupt the formation of the template-monomer complexes in the pre-polymerisation mixture. This condition could lead to lower affinity and selectivity of the imprinted polymers. On the other hand, low initiator concentration would produce less rigid polymers, with poor imprinting sites due to incomplete polymerisation reaction.

Grafting of MIPs onto an inorganic matrix has demonstrated faster binding kinetics, and increased rebinding capacity and selectivity of the hybrid polymers [32]. Once the imprinting sites are located on the surface of the supporting matrix, they would provide faster mass transfer, more accessible sites, and more effective recognition capacity for the template molecules. According to Chen et al. [33], surface functional groups on the silica particles might participate in the formation of the imprinting sites. This could be attributed to the higher binding affinity of the template molecule. However, according to So et al. [34], an excess of unreacted or free silanol groups (Si—OH) on the surface of the silica substrate would result in high non-specific interactions, as well as low imprinting effect.

3.2. Characteristics of polymer particles

FT-IR, SEM, and TEM analyses were performed to confirm a successful polymerisation process. The FT-IR spectra of the CAP, Si, Si@NH_2, and polymer particles are shown in Fig. 1. The characteristic bands of CAP spectra can be attributed to the presence of the benzene ring, nitro, and amide functional groups. The peaks at 1599, 1562, and 1516 cm^{-1} can be attributed to the stretching vibration of CAP benzene ring. The symmetric stretching vibration of the nitro group was

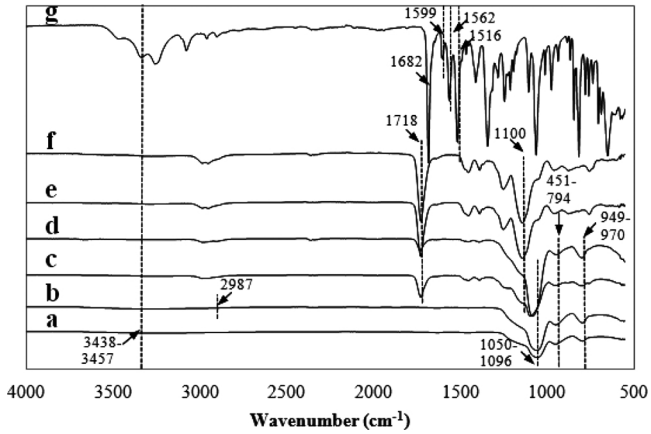

Fig. 1. FT-IR spectra of (a) Si (b) Si@NH_2 (c) Si@MIPs-CAP (d) Si@NIPs-CAP (e) MIPs-CAP (f) NIPs-CAP and (g) CAP.

identified at 1342 cm^{-1}, and the intense peak at 1682 cm^{-1} can be associated with the amide functional group. In the Si spectra, the distinct bands at 1050–1096 cm^{-1} can be linked to the Si—O—Si stretching vibrations, whereas the OH vibrations can be observed at 3438–3457 cm^{-1}. The bands observed at 451–794 cm^{-1} indicated the Si-O vibrations, and the peaks at 949–970 cm^{-1} can be assigned to the silanol groups (Si—OH). The adsorption band at 2987 cm^{-1} observed in the Si@NH_2 spectra can be assigned to C—H bonds, indicating the successful grafting of APTES onto the silica particles [35]. The FT-IR spectra shown in Fig. 1 clearly demonstrate that MIPs-CAP and Si@MIPs-CAP have similar chemical structures with the corresponding NIPs-CAP and Si@NIPs-CAP, respectively. The band at 1718 cm^{-1} can be ascribed to the ester carbonyl groups (C═O) in MAA. Clearly visible bands at 1100 cm^{-1} can be attributed to the stretching vibration of C—O—C ester bond belonging to EDGMA. These spectra show that both the functional monomer (MAA) and the cross-linker (EDGMA) successfully participated in the polymerisation. As for Si@MIPs-CAP and Si@NIPs-CAP, the existence of these two bands in their respective spectra indicated that these polymers were successfully grafted onto the surface of silica particles. The similarity of the shapes and positions of all peaks in the MIPs-CAP and Si@MIPs-CAP spectra with their corresponding NIPs-CAP and Si@NIPs-CAP spectra demonstrated that the template (CAP) had been successfully removed from the imprinted polymers. This observation was confirmed by the absence of three major bands associated with benzene ring, nitro, and amide functional groups in MIPs-CAP and Si@MIPs-CAP spectra.

The morphologies of Si, Si@NH_2, MIPs-CAP, Si@MIPs-CAP, NIPs-CAP, and Si@NIPs-CAP particles were further examined using SEM. The SEM analysis results, as shown in Fig. 2(a,b), reveal that the Si and Si@NH_2 have uniform and spherical shapes. An increase in the diameter of Si@NH_2 particles was expected due to the altered surface properties (with the introduction of amino group) following the modification of silica using APTES. All Si and Si@NH_2 particles have smooth surfaces. On the other hand, the MIPs-CAP and NIPs-CAP particles exhibit irregular spherical shapes with heterogeneous sizes, as seen in Fig. 2(c,d). The surface morphology of MIPs-CAP particles showed minor differences compared to NIPs-CAP particles. However, the NIPs-CAP particles appeared to be smaller than the MIPs-CAP particles. This is due to the addition of CAP template in the reaction mixture, which could have affected particle nucleation and growth during the crosslinking reaction. The Si@MIPs-CAP surface was rougher and denser, which could offer more binding sites for the templates, compared to the surface of Si@NIPs-CAP. TEM analysis results in Fig. 2(g,h) reveal the average particle size of silica at ~378 nm and the larger particle size of Si@MIPs-CAP (~439 nm), as the result of a successful grafting process.

Table 2 provides surface area properties of Si@NH_2, MIPs-CAP, Si@MIPs-CAP, NIPs-CAP, and Si@NIPs-CAP, respectively. N_2 adsorption-

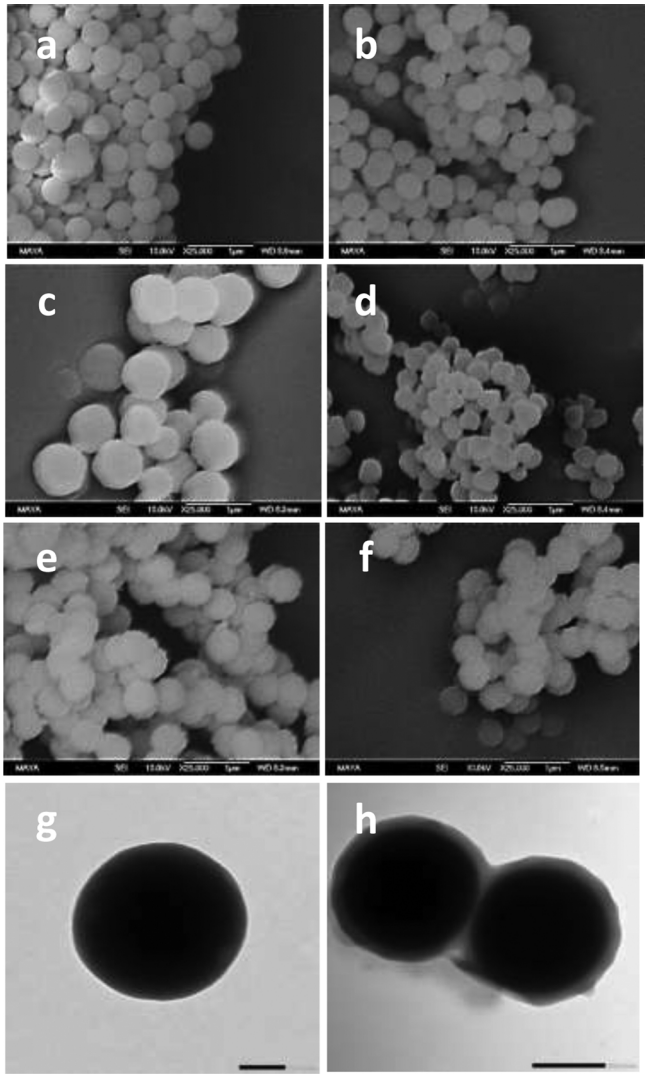

Fig. 2. SEM images (magnifications ×25,000) of (a) Si (b) Si@NH_2 (c) MIPs-CAP (d) NIPs-CAP (e) Si@MIPs-CAP (f) Si@NIPs-CAP and TEM images of (g) Si@NH_2 (magnification ×50,000) (h) Si@MIPs-CAP (magnification × 40,000).

Table 2
BET surface analysis for polymer particles.

Polymer	Surface area ($m^2 g^{-1}$)	Pore volume ($cm^3 g^{-1}$)	Pore size (nm)
MIPs-CAP	8.46	0.024	23.11
NIPs-CAP	21.02	0.088	22.43
Si@MIPs-CAP	58.99	0.189	25.19
Si@NIPs-CAP	41.52	0.106	20.09
Si@NH_2	12.21	0.036	13.09

desorption isotherms for Si@MIPs-CAP, Si@NIPs-CAP, MIPs-CAP, and NIPs-CAP are shown in Fig. 3. According to IUPAC standards, Si@MIPs-CAP and Si@NIPs-CAP have type-II isotherms, with narrow hysteresis loops (type-H3) at relatively higher pressure, which suggests that both core-shell particles have a mixture of mesoporous and macroporous structures. The type-H3 hysteresis loop indicates that the developed pores were slit-shape type or aggregates of plate-like particles [36]. The adsorption and desorption branches of the isotherms for MIPs-CAP and NIPs-CAP were completely overlapping over the whole P/P_0 range. These results show that MIPs-CAP and NIPs-CAP can both be associated with type-I isotherms, suggesting the presence of microporous structures [37]. The data derived from the Barret-Joyner-Halenda (BJH) analysis enabled the determination of the average pore diameter and

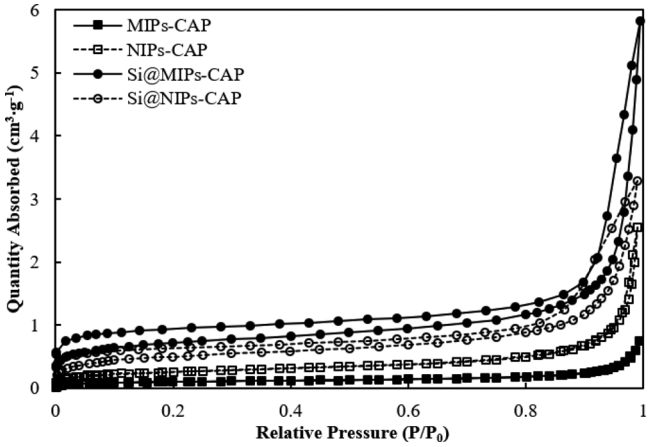

Fig. 3. N_2 adsorption-desorption isotherms of MIPs-CAP, NIPs-CAP, Si@MIPs-CAP and Si@NIPs-CAP at 77K.

cumulative pore volume. The results listed in Table 2 show that all polymers and Si@NH_2 support have average pore diameters that range between 13–25 nm, which are within the mesopore range (2–50 nm). In general, mesopores provide good recognition and desired surface area for interaction with the template molecules. In this study, Si@MIPs-CAP has higher average pore diameter, pore volumes, and specific surface area than MIPs-CAP. This indicates that the silica particles have a significant effect on the porosity and rigidity of the silica-based polymer.

3.3. Rebinding properties of the polymer particles

The effect of different solvents on the rebinding properties of MIPs-CAP, NIPs-CAP, Si@MIPs-CAP, and Si@NIPs-CAP were investigated in an aqueous condition with different volume of acetonitrile. Fig. 4 clearly shows that MIPs-CAP, NIPs-CAP, Si@MIPs-CAP, and Si@NIPs-CAP have higher binding capacities in water compared to in pure acetonitrile. In contrast, the imprinting effect was significantly higher in pure acetonitrile compared to in water. This result was expected because the imprinted polymers possessed the best recognition in the solvent that was used as porogen during the polymerisation reaction [38]. The binding capacity and selectivity of MIPs-CAP were considerably higher than NIPs-CAP in pure acetonitrile. These results confirmed that the binding properties of MIPs-CAP can be attributed to the imprinting process rather than to the surface morphology changes. In the case of silica-based polymers, however, the surface properties were significantly affected by the binding affinity and specificity of the Si@MIPs-CAP. Although both MIPs-CAP and Si@MIPs-CAP displayed

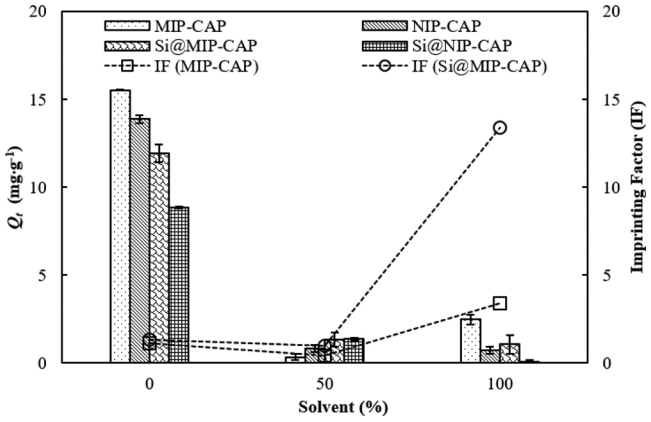

Fig. 4. Adsorption of CAP onto different polymer particles in water containing different amount of acetonitrile (T = 298 K, t = 24 h, C_0 = 100 mg L^{-1}, W = 5 mg).

good imprinting effect in pure acetonitrile, surprisingly, their binding capacities were relatively low. According to Ansell [39], this phenomenon might due to the damaged binding sites upon processing of the materials (grinding and sieving), or to sites collapsing upon template removal, and locally variable swelling of the polymer in a different solvent.

The use of water to substitute organic solvents could greatly weaken non-covalent interactions, such as hydrogen bonding and electrostatic forces, between the template molecules and the binding cavities of the imprinted polymers, thus reducing the molecular recognition ability in aqueous solution [40]. The higher binding capacities displayed by MIPs-CAP, NIPs-CAP, Si@MIPs-CAP, and Si@NIPs-CAP in water could be due to significant hydrophobic interactions, where non-specific adsorption is typically observed. It is well-known that hydrophobic interaction effect is robust in water. The hydrophobicity of imprinted polymers and small organic molecules are largely enhanced in aqueous solutions, which will greatly increase the non-specific hydrophobic interactions between the imprinted polymers and templates, thus increasing the non-specific template binding [40]. When a mixture of acetonitrile/water (50/50) was used, the binding capacities of NIPs-CAP and Si@NIPs-CAP were higher than the binding capacities of MIPs-CAP and Si@MIPs-CAP. These results showed that adding water would decrease the specific binding effect of MIPs-CAP and Si@MIPs-CAP. This could be due to the strong polarity of water, which could easily disrupt the hydrogen bonds between the imprinted polymers and template molecules. Furthermore, MIPs synthesised in organic solutions often show poor dispersion and a different swelling effect in aqueous solutions, which would impede the access of template molecules to the recognition cavities [41].

Another highlight from this study is the comparisons of binding affinity and imprinting effect between silica-composite and organic-based polymers. The imprinting effect of Si@MIPs-CAP was more pronounced compared to MIPs-CAP, both in water and pure acetonitrile. This result suggested that the amino-functionalised silica particles have a significant impact on the molecular recognition of Si@MIPs-CAP. From the BET analysis results, the higher specific surface area of Si@MIPs-CAP contributed to the higher amount of the resultant imprinting cavities. However, the high specific surface area of Si@MIPs-CAP showed less effect on its binding capacity towards CAP as compared to MIPs-CAP. According to Goscianska et al. [42] and Yokai et al. [43], the high density of functional groups on the surface might prevent the diffusion of molecules in the mesopores thus affecting the performance of the material. A control experiment was conducted using Si@NH_2 to verify that the binding capacities of the silica-based polymers were contributed by the imprinting process, and not due to silica adsorption. From the results shown in Fig. 5, the binding capacity of Si@NH_2 on CAP is considerably low and insignificant. At the pH studied (pH 7), the

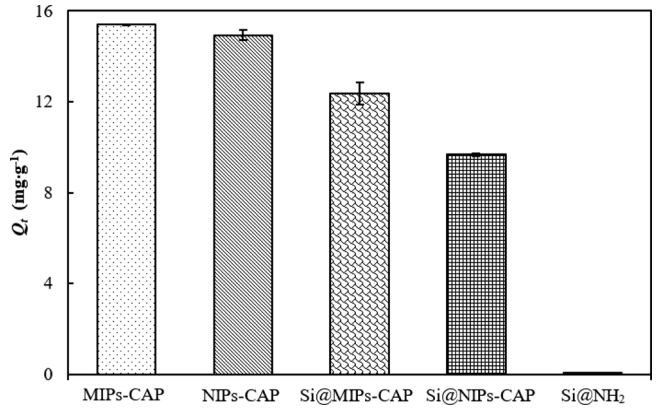

Fig. 5. Adsorption of CAP onto amino-functionalised silica particles in water as comparison with other polymer particles (pH = 7, T = 298 K, t = 24 h, C_0 = 100 mg L^{-1}, W = 5 mg).

Si@NH_2 (pI of 9.7) and the CAP (pK_a of 8.69) would become positively charged due to the protonation of the amine groups (–NH_3^+) over the surface Due to the electrostatic repulsion between the positively charged functional groups of the Si@NH_2 and the CAP, the binding capacities of the silica material would decrease. This result also indicated that the presence of -NH_2 over the surface of the silica upon functionalisation and the free −Si−OH promoted the formation of the imprinting sites rather than disturbing the template-monomer assemblies during the polymerisation reaction [33].

The effects of solution pH on the binding capacities of MIPs-CAP, NIPs-CAP, Si@MIPs-CAP, and Si@NIPs-CAP were investigated at different initial pH values (2–9). Solution pH is an important parameter to study because it could influence the surface charge of the polymers and affect the ionisation form of the antibiotic [44]. The pK_a values of MAA and CAP were 4.66 and 8.69, respectively. When the pH of the solution is lower than the pK_a values, the −COOH group in the MAA, and the −NH and −OH groups in the CAP would be protonated and presented as cations (−$COOH_2^+$, −NH_2^+, and −OH_2^+). However, the binding capacity of the polymers might also be due to the hydrophobic effect and electrostatic interaction between −$COOH_2^+$ and the nitro group in CAP. When the pH of the solution is higher than the pK_a value of the MAA, the carboxylic groups over the polymer's surface would become negatively charged (−COO^-), while the CAP would remain positively charged. This condition would increase the electrostatic interaction between the charged functional groups, thus increasing the binding capacity of the polymers. Similarly, at solution pH of higher than the pK_a value of the CAP, the antibiotic would become negatively charged because of the deprotonation of the amide group (−N^-). Owing to the electrostatic repulsion between the negatively charged functional groups of the MAA and the CAP, the binding capacities of the polymers would decrease.

In this study, the binding capacities between the MIPs-CAP and NIPs-CAP showed no significant difference at all pH, which decreased the values of the imprinting factor (IF). However, a different scenario was observed for silica-based polymers. As shown in Fig. 6, the IF values of Si@MIPs-CAP are significantly higher than the IF values of MIPs-CAP, indicating that the imprinting effect has a stronger influence on the silica-based polymer. It was also observed that the IF values of Si@MIPs-CAP were relatively higher between pH 4 and 5, and between pH 8 and 9. These results showed that molecular recognition was stronger when the solution pH was closer to the pK_a values of the MAA and CAP, which promoted the formation of hydrogen bonds between the carboxylic and amide functional groups. However, when the pH of the solution was lower or higher than the pK_a values, the IF values were decreased. The protonation and deprotonation of the carboxylic and the amide functional groups have impeded the formation of hydrogen bonds, thus decreasing the molecular recognition of the imprinting sites for CAP.

3.4. Adsorption kinetics

The adsorption capacities of CAP (100 mg/L) for Si@MIPs-CAP, Si@NIPs-CAP, MIPs-CAP, and NIPs-CAP are investigated and the data are plotted, as shown in Fig. 7. Results showed that for all polymer particles, the adsorption capacity increased rapidly in the first 20 min, and then began to slow down with the remaining contact times as it approached equilibrium. The rapid solute uptake at the beginning of the adsorption process could be due to the high concentration gradient between the adsorbent and the adsorbate in the solution, as well as the abundantly available vacant sites. After a certain time, the remaining vacant sites became difficult to occupy due to the repulsion force between the adsorbates on the surface of the adsorbent. The solute uptake occurred gradually until it reached equilibrium when the solution concentration was decreased. The adsorption equilibrium for both Si@MIPs-CAP and MIPs-CAP was achieved at a contact time of 80 min, which was faster than the time taken by Si@NIPs-CAP and NIPs-CAP,

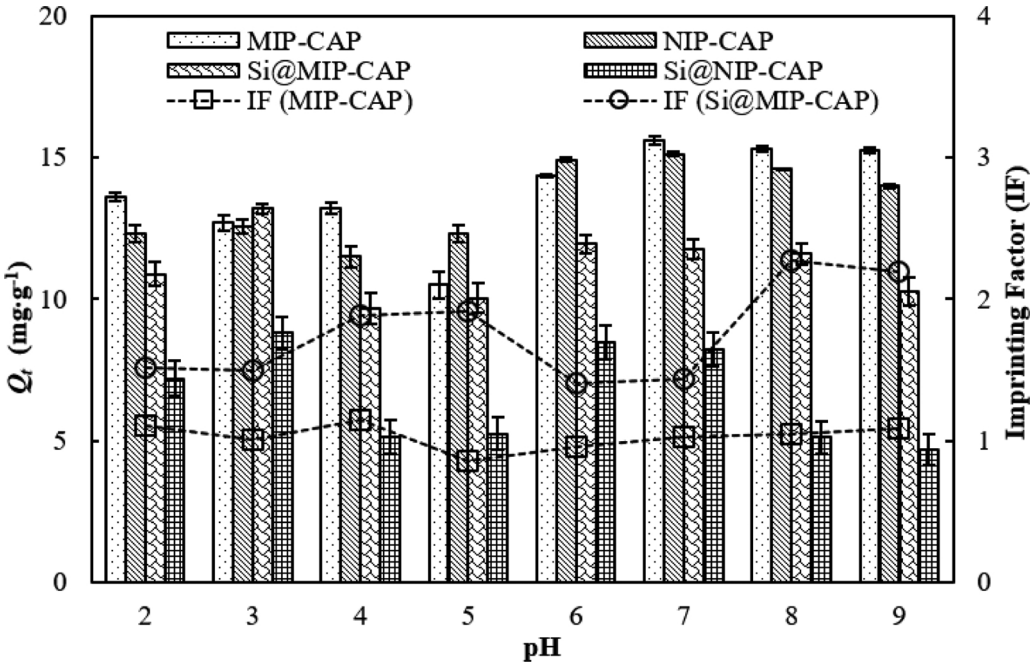

Fig. 6. Effect of pH solution on adsorption of CAP onto different polymer particles (T = 298 K, t = 24 h, C_0 = 100 mg L^{-1}, W = 5 mg).

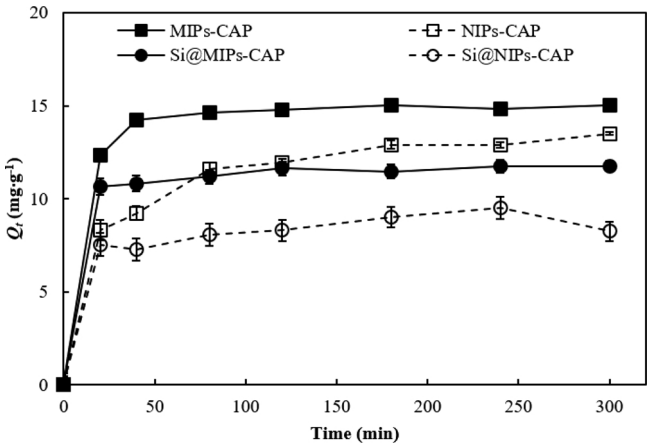

Fig. 7. Equilibrium profiles of CAP adsorption onto different polymer particles in water (pH = 8, T = 298 K, C_0 = 100 mg L^{-1}, W = 5 mg).

both at 180 min. Fig. 7 also shows that the adsorption capacities of imprinted polymer particles were higher than their respective counterparts. The higher binding capacity can be attributed to specific imprinting sites in both Si@MIPs-CAP and MIPs-CAP, and thus, they have stronger affinity towards CAP than Si@NIPs-CAP and NIPs-CAP, respectively.

To understand the rate of CAP uptake by the polymer particles during the adsorption process, experimentally obtained kinetics adsorption data were fitted to the pseudo-first order, pseudo-second order, Elovich, and Weber-Morris intra-particle diffusion models. The kinetic parameters obtained from the models are tabulated and compared, as shown in Table 3. The R^2 values were found to be more than 0.98 for all polymer particles, indicating that the pseudo-second order model fitted the experimental data better compared to pseudo-first order and Elovich models. Therefore, the adsorption rates of CAP were controlled mainly by chemical adsorption [45]. The α values that were determined from the Elovich model showed that Si@MIPs-CAP (1.2×10^9 mg g^{-1} min^{-1}) have higher initial sorption rates compared to the α values of MIPs-CAP (2.2×10^5 mg g^{-1} min^{-1}). These results justified the incorporation of silica particles in preparing core-shell imprinted polymer particles, which demonstrated faster binding kinetics. Once the imprinting sites were located on the surface of the supporting matrix, they would provide faster mass transfer, more accessible sites, and more effective recognition capacity for the template molecules [46]. The Weber-Morris intra-particle diffusion plots, as shown in Fig. 8, are used to determine whether external diffusion or intra-particle diffusion is the rate-limiting step. Since the intra-particle diffusion plot did not pass through the origin, this model has indicated that the adsorption mechanism was governed by more than one mechanism, and that intra-particle diffusion was not the predominant step [47]. It could be assumed that external mass transfer was significant only in the early stages of adsorption, and then proceeded with the gradual adsorption stage controlled by intraparticle diffusion [48].

3.5. Adsorption isotherms

The experimental data for the adsorption of CAP onto different polymer particles (Si@MIPs-CAP, MIPs-CAP, Si@NIPs-CAP, and NIPs-CAP) were fitted to Langmuir, Freundlich, Temkin, and Dubinin–Radushkevich isotherm models. The adsorption isotherm parameters are tabulated in Table 4. For Si@MIPs-CAP (R^2 = 0.9991) and Si@NIPs-CAP (R^2 = 0.9872), the data fitted well with Langmuir model. These results indicated the monolayer adsorption of CAP onto the surface of Si@MIPs-CAP and Si@NIPs-CAP, with uniformly distributed binding sites [49]. According to Ansell [39], the number of selective sites and their binding affinities of the target molecule with the MIPs could be determined from the parameters in Langmuir isotherms. The distribution of the binding site affinity could be classified from strong (favourable) and selective sites present in small numbers to weaker (less favourable) and less selective sites present at far greater densities. Therefore, for a single solute adsorption system, the separation factor, R_L, could be used as a relative indicator to determine the binding site selectivity of the solute to the respective adsorbent. Based on R_L values in Table 4, Si@MIPs-CAP (imprinted) have shown higher affinity to CAP than their non-imprinted counterparts, NIPs-CAP and Si@NIPs-CAP. The value of R_L, for Si@MIPs-CAP was significantly lower than MIPs-CAP which indicates that the binding affinity of CAP towards the selective sites of Si@MIPs-CAP was more favourable at higher initial concentrations [50]. The preparation mechanism of the

Table 3
Kinetic parameters of CAP adsorption onto polymer particles.

Models	Parameters	MIPs-CAP	NIPs-CAP	Si@MIPs-CAP	Si@NIPs-CAP
Pseudo-first order	Q_e (mg g^{-1})	1.8147	6.1935	1.6815	3.4429
	k_1 (min^{-1})	0.0062	0.0052	0.0039	0.0084
	R^2	0.7723	0.9163	0.8400	0.8194
	SSE	0.5916	0.5980	0.1508	0.5412
Pseudo-second order	Q_e (mg g^{-1})	15.175	14.144	11.905	8.9206
	k_2 (mg min^{-1})	0.0196	0.0038	0.0213	0.0222
	R^2	0.9998	0.9987	0.9999	0.9881
	SSE	0.2743	0.4381	0.2815	0.5042
Elovich	α (mg g^{-1} min^{-1})	2.2×10^{5}	1.6915	1.2×10^{9}	8.3×10^{2}
	β (g mg^{-1})	0.8593	1.9761	0.4574	0.7498
	R^2	0.7874	0.9689	0.9821	0.8853
	SSE	0.4259	0.3231	0.1093	0.4609
Weber–Morris intra-particle diffusion	$k_{1,1}$ (mg g^{-1} min$^{-1/2}$)	0.4870	0.7530	0.1299	0.1805
	I_1 (mg g^{-1})	10.515	4.7617	10.028	6.4343
	R^2	0.8052	0.9777	0.9942	0.9917
	SSE	2.1284	2.2717	0.2603	0.5371
	$k_{1,2}$ (mg g^{-1} min$^{-1/2}$)	0.0515	0.2230	0.0614	0.0510
	I_2 (mg g^{-1})	14.171	9.6214	10.802	7.6392
	R^2	0.9339	0.9434	0.9973	0.8645
	SSE	0.7950	1.1180	0.2457	0.5786

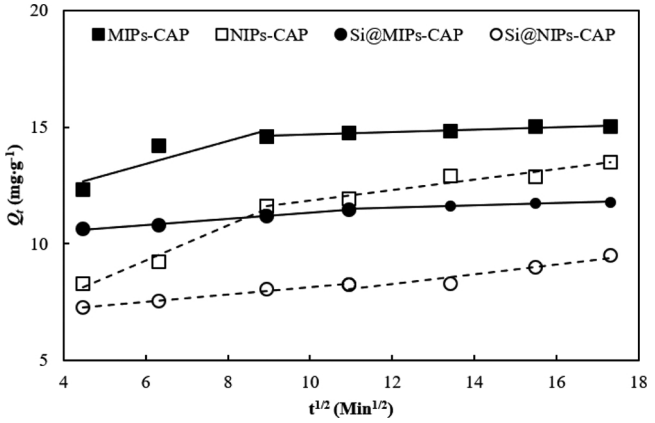

Fig. 8. Intra-particle diffusion kinetic model plots of MIPs-CAP, NIPs-CAP, Si@MIPs-CAP and Si@NIPs-CAP.

MIPs could affect molecular recognition of the adsorbents and the adsorption capacity. As for MIPs-CAP, a conventional molecularly imprinting method typically produced materials of thick morphology, irregular shape, and heterogeneous binding sites distribution that could contribute to the lower affinity of the target molecules to the recognition sites [51]. The thick MIP layer provides higher mass transfer resistance leading to the restriction or no access for the target molecule to bind on the recognition sites. The positive values of Gibbs free energy ($\Delta G°$) calculated using Langmuir constant, K_L indicated that the adsorption processes were non-spontaneous at temperature of 298 K. On the other hand, MIPs-CAP (R^2 = 0.9998) and NIPs-CAP (R^2 = 0.9931) showed higher correlations with the Freundlich model. This result indicated a multilayer adsorption of CAP with heterogeneous binding sites. The values of n for both MIPs-CAP and NIPs-CAP were higher than 1, indicating favourable adsorption [52]. This result showed that the surface functionalisation of silica nanoparticles has significantly affected the conformation of binding sites on the imprinted polymers. Silica would marginally swell in the presence of solvents, which permits it to maintain the shape and size of its imprinting sites. According to Wan et al. [46], immobilising functional monomers on core particles is helpful to control the homogeneity of the binding sites and discuss the mechanism of molecular imprinting. The Temkin model showed a good fit ($R^2 > 0.9$) with the experimental data and could be used to describe

Table 4
Isotherm parameters of CAP adsorption onto polymer particles.

Models	Parameters	MIPs-CAP	NIPs-CAP	Si@MIPs-CAP	Si@NIPs-CAP
Langmuir	Q_{max} (mg g^{-1})	68.027	62.500	32.258	29.586
	K_L (L mg^{-1})	0.0187	0.0172	0.0180	0.0112
	R_L	0.1785	0.1482	0.0642	0.1554
	$\Delta G°$ (kJ mol^{-1})	9.8588	10.066	9.9534	11.129
	R^2	0.9623	0.9487	0.9991	0.9872
	SSE	2.4019	2.3921	0.4063	0.8862
Freundlich	K_f [(mg g^{-1})(L mg^{-1})$^{1/n}$)]	3.2696	3.1175	2.0654	1.2246
	N	1.8044	1.8741	2.0938	1.8832
	R^2	0.9998	0.9931	0.9574	0.9636
	SSE	0.1836	0.9186	2.1891	1.7980
Temkin	β (J mol^{-1})	13.116	11.702	7.0514	6.5886
	b_T	185.82	208.28	345.64	369.92
	K_T (L g^{-1})	0.2947	0.2457	0.1746	0.1082
	R^2	0.9419	0.9233	0.9904	0.9710
	SSE	3.8621	4.0493	0.7484	1.1084
Dubinin-Radushkevich	Q_{max} (mg g^{-1})	30.966	28.341	20.920	17.214
	β (mol^{-2}J^{-2})	1.0×10^{-5}	9.0×10^{-6}	5.0×10^{-5}	9.0×10^{-5}
	E (J mol^{-1})	0.2236	0.2357	0.1000	0.0795
	R^2	0.6983	0.6696	0.8448	0.7875
	SSE	11.203	10.698	3.7433	3.5522

Table 5
Comparative CAP adsorption capacities in aqueous phase.

Adsorbent	Q_{max} (mg g^{-1})	IF	Reference
BC (Bamboo charcoal)	8.1	–	[53]
MMIPs	17	1.52	[51]
MMSNs@MIPs	41.7	1.13	[21]
HMINs-2	184.6	1.88	[54]
MMINs	25.87	2.69	[55]
MIP	14.73	4.77	[56]
fBc (AC from eucalyptus wood biomass)	21.35	–	[57]
CAP-MIPMs	18.46	1.53	[58]
Si@MIPs-CAP	32.26	2.27	This work

the mechanism of CAP adsorptions. From Table 4, the smaller values of β (J mol^{-1}) confirmed that the adsorptions were physically governed. These values suggested that the interactions between CAP and the polymer particles were mainly hydrogen bonds, van der Waals forces, electrostatic forces, and hydrophobic interaction. The constant of Temkin b_T greater than 1 determined from the studies indicated that the adsorption processes were exothermic in nature [50]. The R^2 values of the Dubinin-Radushkevich model were the lowest compared to the R^2 values of the other isotherm models, and it was poorly fitted to the experimental data. This model was not applicable enough to support the adsorption mechanism. Thus, it was excluded from further discussion.

3.6. Comparative adsorption performance study

The adsorption performance of CAP onto Si@MIPs-CAP was compared with other MIPs adsorbents previously reported in the literature, as listed in Table 5. The comparison was made based on Langmuir's maximum monolayer adsorption capacity (Q_{max}) and imprinting factor (IF). The Si@MIPs-CAP prepared in this study exhibited higher adsorption of CAP and higher IF values compared with other reported absorbents. The MIPs adsorbents prepared using traditional imprinting methods (MMIPs, MMINs, MIP, and CAP-MIPMs) displayed low adsorption capacities. The active recognition sites are normally embedded deep in the MIPs particles, which would limit their mass transfer efficiency. The highest Q_{max} (184.6 mg g^{-1}) for CAP adsorption by MIPs adsorbent was reported using HMINs-2, a type of hollow imprinted polymer nanorods. However, it has a low specific recognition (IF = 1.88) compared to Si@MIPs-CAP (IF = 2.27). The closest comparison can be made with MMSNs@MIPs, a mesoporous silica-containing hybrid MIPs, with Q_{max} of 41.7 mg g^{-1}, which was slightly higher than the Q_{max} of Si@MIPs-CAP. However, its IF value (1.13) was significantly lower than the IF value of Si@MIPs-CAP. Si@MIPs-CAP also showed better CAP adsorption compared to bamboo charcoal, BC and activated carbon derived from plant-based biomass, fBc.

4. Conclusion

This study has successfully demonstrated that Si@NH_2 core nanoparticles have significantly affected the material characteristics and adsorption behaviours of Si@MIPs-CAP. The silica core-shell molecularly imprinted polymer particles, Si@MIPs-CAP have demonstrated higher binding affinity to CAP than their non-imprinted counterparts, NIPs-CAP and Si@NIPs-CAP. Thus, Si@MIPs-CAP has the potential to be an efficient water-compatible adsorbent for CAP removal in aqueous phase.

CRediT authorship contribution statement

Z. Mohamed Idris: Funding acquisition, Investigation, Writing - original draft. **B.H. Hameed:** Writing - review & editing. **L. Ye:** Resources, Supervision. **S. Hajizadeh:** Supervision, Writing - review & editing. **B. Mattiasson:** Writing - review & editing. **A.T. Mohd Din:** Project administration, Funding acquisition, Supervision, Writing - review & editing.

Declaration of competing interest

The authors declare that they have no known competing financial interests or personal relationships that could have appeared to influence the work reported in this paper.

Acknowledgements

This work was partly supported by the World Bank Robert S. McNamara Fellowship Program and the Ministry of Higher Education Malaysia through the Fundamental Research Grant Scheme (6071330). The authors are grateful to the Division of Pure and Applied Biochemistry, Lund University, Sweden and to School of Chemical Engineering, Universiti Sains Malaysia for supporting and providing laboratory facilities.

Appendix A. Supplementary data

Supplementary material related to this article can be found, in the online version, at doi:https://doi.org/10.1016/j.jece.2020.103981.

References

[1] F.S. Freyria, F. Geobaldo, B. Bonelli, Nanomaterials for the abatement of pharmaceuticals and personal care products from wastewater, Appl. Sci. 8 (2) (2018) 170, https://doi.org/10.3390/app8020170.
[2] A.J. Ebele, M. Abou-Elwafa Abdallah, S. Harrad, Pharmaceuticals and personal care products (PPCPs) in the freshwater aquatic environment, Emerg. Contam. 3 (1) (2017) 1–16, https://doi.org/10.1016/j.emcon.2016.12.004.
[3] M.E. Falagas, A.P. Grammatikos, A. Michalopoulos, Potential of old-generation antibiotics to address current need for new antibiotics, Expert Rev. Anti Infect. Ther. 6 (5) (2008) 593–600, https://doi.org/10.1586/14787210.6.5.593.
[4] J.A. Turton, C.M. Andrews, A.C. Havard, T.C. Williams, Studies on the haemotoxicity of chloramphenicol succinate in the Dunkin Hartley guinea pig, Int. J. Exp. Pathol. 83 (5) (2002) 225–238.
[5] S. Marni, M.R. Marzura, A.E. Afandi, A.K. Suliana, Veterinary drug residues in chicken, pork and beef in Peninsular Malaysia in the period 2010–2016, Mal. J. Vet. Res. 8 (2) (2017) 71–77.
[6] Fifteenth A Schedule - Table II Prohibited Drugs: Malaysia Food Regulations, (1985) (accessed 6 May 2019), http://fsq.moh.gov.my.
[7] K.H. Ng, L. Samuel, M.M. Kathleen, S.S. Leong, C. Felecia, Distribution and prevalence of chloramphenicol-resistance gene in *Escherichia coli* isolated from aquaculture and other environment, Int. Food Res. J. 21 (4) (2014) 1321–1325.
[8] B. Mattiasson, G. Ertürk, Molecularly imprinted polymers: the affinity adsorbents for environmental biotechnology, Chapter 8, in: A. Tiwari, L. Uzun (Eds.), Advanced Molecularly Imprinting Materials, John Wiley and Sons Inc., 2016, pp. 327–351, , https://doi.org/10.1002/9781119336181.ch8.
[9] L. Sun, J. Guan, Q. Xu, X. Yang, J. Wang, X. Hu, Synthesis and applications of molecularly imprinted polymers modified TiO_2 nanomaterials: a review, Polymers 10 (11) (2018) 1248, https://doi.org/10.3390/polym10111248.
[10] X. Wang, Y. Zhou, Y. Niu, S. Zhao, B. Gong, Preparation of monodisperse enrofloxacin molecularly imprinted polymer microspheres and their recognition characteristics, Int. Anal. Chem. 2019 (2019) 5970754, , https://doi.org/10.1155/2019/5970754.
[11] Y. Ren, W. Ma, J. Ma, Q. Wen, J. Wang, F. Zhao, Synthesis and properties of bisphenol a molecular imprinted particle for selective recognition of BPA from water, J. Colloid Interface Sci. 367 (1) (2012) 355–361, https://doi.org/10.1016/j.jcis.2011.10.009.
[12] L. Chen, S. Xu, J. Li, Recent advances in molecular imprinting technology: current status, challenges and highlighted applications, Chem. Soc. Rev. 40 (5) (2011) 2922–2942, https://doi.org/10.1039/C0CS00084A.
[13] M. Niu, C. Pham-Huy, H. He, Core-shell nanoparticles coated with molecularly imprinted polymers: a review, Microchim. Acta 183 (10) (2016) 2677–2695, https://doi.org/10.1007/s00604-016-1930-4.
[14] L. Zhao, F. Zhao, B. Zeng, Synthesis of water-compatible surface-imprinted polymer via click chemistry and RAFT precipitation polymerization for highly selective and sensitive electrochemical assay of fenitrothion, Biosens. Bioelectron. 62 (2014) 19–24, https://doi.org/10.1016/j.bios.2014.06.022.
[15] E. Moczko, A. Guerreiro, E. Piletska, S. Piletsky, PEG-stabilized core–shell surface-imprinted nanoparticles, Langmuir 29 (31) (2013) 9891–9896, https://doi.org/10.1021/la401891f.
[16] H.T. Fan, W. Sun, B. Jiang, Q.J. Wang, D.W. Li, C.C. Huang, K.J. Wang, Z.G. Zhang, W.X. Li, Adsorption of antimony(III) from aqueous solution by mercapto-

functionalized silica-supported organic–inorganic hybrid sorbent: mechanism insights, Chem. Eng. J. 286 (2016) 128–138, https://doi.org/10.1016/j.cej.2015.10.048.
[17] M. Zhao, X. Ma, F. Zhao, H. Guo, Molecularly imprinted polymer silica monolith for the selective extraction of alpha-cypermethrin from soil samples, J. Mater. Sci. 51 (7) (2016) 3440–3447, https://doi.org/10.1007/s10853-015-9661-1.
[18] A. Mehdinia, S. Dadkhah, T. Baradaran Kayyal, A. Jabbari, Design of a surface-immobilized 4-nitrophenol molecularly imprinted polymer via pre-grafting amino functional materials on magnetic nanoparticles, J. Chromatogr. A 1364 (2014) 12–19, https://doi.org/10.1016/j.chroma.2014.08.058.
[19] L. Jiang, H. Bagán, T. Kamra, T. Zhou, L. Ye, Nanohybrid polymer brushes on silica for bioseparation, J. Mater. Chem. B 4 (19) (2016) 3247–3256, https://doi.org/10.1039/C6TB00241B.
[20] L. Ye, R. Weiss, K. Mosbach, Synthesis and characterization of molecularly imprinted microspheres, Macromolecules 33 (22) (2000) 8239–8245, https://doi.org/10.1021/ma000825t.
[21] J. Dai, J. He, A. Xie, L. Gao, J. Pan, X. Chen, Z. Zhou, Z. Wei, Y. Yan, Novel pitaya-inspired well-defined core–shell nanospheres with ultrathin surface imprinted nanofilm from magnetic mesoporous nanosilica for highly efficient chloramphenicol removal, Chem. Eng. J. 284 (2016) 812–822, https://doi.org/10.1016/j.cej.2015.09.050.
[22] S.H. Chien, W.R. Clayton, Application of Elovich equation to the kinetics of phosphate release and sorption in soils 1, Soil Sci. Soc. Am. J. 44 (2) (1980) 265–268, https://doi.org/10.2136/sssaj1980.03615995004400020013x.
[23] W.J. Weber, J.C. Morris, Advances in water pollution research: removal of biologically resistant pollutant from waste water by adsorption, Proceedings of International Conference on Water Pollution Symposium, 2, Pergamon Press, Oxford UK, 1962, pp. 231–266.
[24] S. Langergren, B.K. Svenska, Zur theorie der sogenannten adsorption geloester stoffe, Vaternskapsakad Handlingar 24 (4) (1898) 1–39.
[25] M.M. Dubinin, L.V. Radushkevich, The equation of the characteristic curve of the activated charcoal, Proc. Acad. Sci. Phys. Chem. Sect. 55 (1947) 331–337.
[26] M.I. Temkin, V. Pyzhev, Kinetics of ammonia synthesis on promoted iron catalyst, Acta Phys. Chim. USSR 12 (1940) 327–356.
[27] I. Langmuir, The constitution and fundamental properties of solids and liquids, J. Am. Chem. Soc. 38 (11) (1916) 2221–2295, https://doi.org/10.1021/ja02268a002.
[28] H.M.F. Freundlich, Over the adsorption in solution, J. Phys. Chem. 57 (1906) 385–471.
[29] A.M. Chrzanowska, A. Poliwoda, P.P. Wieczorek, Characterization of particle morphology of biochanin a molecularly imprinted polymers and their properties as a potential sorbent for solid-phase extraction, Mater. Sci. Eng., C 49 (2015) 793–798, https://doi.org/10.1016/j.msec.2015.01.069.
[30] P. Luliński, D. Maciejewska, Impact of functional monomers, cross-linkers and porogens on morphology and recognition properties of 2-(3,4-dimethoxyphenyl) ethylamine imprinted polymers, Mater. Sci. Eng. C 31 (2) (2011) 281–289, https://doi.org/10.1016/j.msec.2010.09.010.
[31] Z. Ren, D. Kong, K. Wang, W. Zhang, Preparation and adsorption characteristics of an imprinted polymer for selective removal of Cr(VI) ions from aqueous solutions, J. Mater. Chem. A 2 (42) (2014) 17952–17961, https://doi.org/10.1039/C4TA03024A.
[32] H. Chen, D. Yuan, Y. Li, M. Dong, Z. Chai, J. Kong, G. Fu, Silica nanoparticle supported molecularly imprinted polymer layers with varied degrees of crosslinking for lysozyme recognition, Anal. Chim. Acta 779 (2013) 82–89, https://doi.org/10.1016/j.aca.2013.03.052.
[33] H. Chen, J. Kong, D. Yuan, G. Fu, Synthesis of surface molecularly imprinted nanoparticles for recognition of lysozyme using a metal coordination monomer, Biosens. Bioelectron. 53 (2014) 5–11, https://doi.org/10.1016/j.bios.2013.09.037.
[34] J. So, C. Pang, H. Dong, P. Jang, U, J, K. Ri, C. Yun, Adsorption of 1-naphthyl methyl carbamate in water by utilizing a surface molecularly imprinted polymer, Chem. Phys. Lett. 699 (2018) 199–207, https://doi.org/10.1016/j.cplett.2018.03.059.
[35] W.R. Zhao, T.F. Kang, L.P. Lu, S.Y. Cheng, Magnetic surface molecularly imprinted poly(3-aminophenylboronic acid) for selective capture and determination of diethylstilbestrol, RSC Adv. 8 (24) (2018) 13129–13141, https://doi.org/10.1039/C8RA01250D.
[36] K. Golker, I.A. Nicholls, The effect of crosslinking density on molecularly imprinted polymer morphology and recognition, Eur. Polym. J. 75 (2016) 423–430, https://doi.org/10.1016/j.eurpolymj.2016.01.008.
[37] J.G. Wang, H. Liu, H. Sun, W. Hua, H. Wang, X. Liu, B. Wei, One-pot synthesis of nitrogen-doped ordered mesoporous carbon spheres for high-rate and long-cycle life supercapacitors, Carbon 127 (2018) 85–92, https://doi.org/10.1016/j.carbon.2017.10.084.
[38] X.H. Wang, L.F. Xie, Q. Dong, H.L. Liu, Y.P. Huang, Z.S. Liu, Synthesis of monodisperse molecularly imprinted microspheres with multi-recognition ability via precipitation polymerization for the selective extraction of cyromazine, melamine, triamterene and trimethoprim, J. Chromatogr. B 1007 (2015) 127–131, https://doi.org/10.1016/j.jchromb.2015.11.009.
[39] R.J. Ansell, Characterization of the binding properties of molecularly imprinted polymers, Adv. Biochem. Engin./Biotechnol. 250 (2015) 51–93, https://doi.org/10.1007/10_2015_316.
[40] H. Zhang, Water-compatible molecularly imprinted polymers: promising synthetic substitutes for biological receptors, Polymer 55 (3) (2014) 699–714, https://doi.org/10.1016/j.polymer.2013.12.064.
[41] S. Pardeshi, R. Dhodapkar, A. Kumar, Influence of porogens on the specific recognition of molecularly imprinted poly(acrylamide-co-ethylene glycol dimethacrylate), Compos. Interfaces 21 (1) (2014) 13–30, https://doi.org/10.1080/15685543.2013.830515.
[42] J. Goscianska, A. Olejnik, I. Nowak, APTES-functionalized mesoporous silica as a vehicle for antipyrine – adsorption and release studies, Colloids Surface A 533 (2017) 187–196, https://doi.org/10.1016/j.colsurfa.2017.07.043.
[43] T. Yokai, Y. Kubota, T. Tatsumi, Amino-functionalized mesoporous silica as base catalyst and adsorbent, Appl. Catal. A 421-422 (2012) 14–37, https://doi.org/10.1016/j.apcata.2012.02.004.
[44] Y. Li, J. Zhang, H. Liu, Removal of chloramphenicol from aqueous solution using low-cost activated carbon prepared from *Typha orientalis*, Water 10 (4) (2018) 351, https://doi.org/10.3390/w10040351.
[45] K.C. Bedin, A.C. Martins, A.L. Cazetta, O. Pezoti, V.C. Almeida, KOH-activated carbon prepared from sucrose spherical carbon: adsorption equilibrium, kinetic and thermodynamic studies for methylene blue removal, Chem. Eng. J. 286 (2016) 476–484, https://doi.org/10.1016/j.cej.2015.10.099.
[46] L. Wan, Z. Chen, C. Huang, X. Shen, Core-shell molecularly imprinted particles, TrAC Trends Anal. Chem. 95 (2017) 110–121, https://doi.org/10.1016/j.trac.2017.08.010.
[47] S.A. Drweesh, N.A. Fathy, M.A. Wahba, A.A. Hanna, A.I.M. Akarish, E.A.M. Elzahany, I.Y. El-Sherif, K.S. Abou-El-Sherbini, Equilibrium, kinetic and thermodynamic studies of Pb(II) adsorption from aqueous solutions on HCl-treated Egyptian kaolin, J. Environ. Chem. Eng. 4 (2) (2016) 1674–1684, https://doi.org/10.1016/j.jece.2016.02.005.
[48] V. Fierro, V. Torné-Fernández, D. Montané, A. Celzard, Adsorption of phenol onto activated carbons having different textural and surface properties, Microporous Mesoporous Mater. 111 (1–3) (2008) 276–284, https://doi.org/10.1016/j.micromeso.2007.08.002.
[49] S. Rangabhashiyam, N. Selvaraju, Evaluation of the biosorption potential of a novel Caryota urens inflorescence waste biomass for the removal of hexavalent chromium from aqueous solutions, J. Taiwan Inst. Chem. Eng. 47 (2015) 59–70, https://doi.org/10.1016/j.jtice.2014.09.034.
[50] L. Zhang, Y. Wang, S. Jin, Q. Lu, J. Ji, Adsorption isotherm, kinetic and mechanism of expanded graphite for sulfadiazine antibiotics removal from aqueous solutions, Environ. Technol. 38 (20) (2017) 2629–2638, https://doi.org/10.1080/09593330.2016.1272637.
[51] W. Ma, J. Dai, X. Dai, Z. Da, Y. Yan, Core-shell molecularly imprinted polymers based on magnetic chitosan microspheres for chloramphenicol selective adsorption, Monatsh. Chem. 146 (3) (2015) 465–474, https://doi.org/10.1007/s00706-014-1351-1.
[52] K. Shahul Hameed, P. Muthirulan, M. Meenakshi Sundaram, Adsorption of chromotrope dye onto activated carbons obtained from the seeds of various plants: equilibrium and kinetics studies, Arab. J. Chem. 10 (2017) S2225–S2233, https://doi.org/10.1016/j.arabjc.2013.07.058.
[53] P. Liao, Z. Zhan, J. Dai, X. Wu, W. Zhang, K. Wang, S. Yuan, Adsorption of tetracycline and chloramphenicol in aqueous solutions by bamboo charcoal: a batch and fixed-bed column study, Chem. Eng. J. 228 (2013) 496–505, https://doi.org/10.1016/j.cej.2013.04.118.
[54] A. Xie, J. Dai, X. Chen, T. Zou, J. He, Z. Chang, C. Li, Y. Yan, Hollow imprinted polymer nanorods with a tunable shell using halloysite nanotubes as a sacrificial template for selective recognition and separation of chloramphenicol, RSC Adv. 6 (56) (2016) 51014–51023, https://doi.org/10.1039/C6RA08042A.
[55] J. He, T. Zou, X. Chen, J. Dai, A. Xie, Z. Zhou, Y. Yan, Magnetic organic–inorganic nanocomposite with ultrathin imprinted polymers via an in situ surface-initiated approach for specific separation of chloramphenicol, RSC Adv. 6 (74) (2016) 70383–70393, https://doi.org/10.1039/C6RA17258J.
[56] Y. Xie, M. Zhao, Q. Hu, Y. Cheng, Y. Guo, H. Qian, W. Yao, Selective detection of chloramphenicol in milk based on a molecularly imprinted polymer-surface-enhanced Raman spectroscopic nanosensor, J. Raman Spectrosc. 48 (2) (2017) 204–210, https://doi.org/10.1002/jrs.5034.
[57] M.B. Ahmed, J.L. Zhou, H.H. Ngo, W. Guo, M.A.H. Johir, D. Belhaj, Competitive sorption affinity of sulfonamides and chloramphenicol antibiotics toward functionalized biochar for water and wastewater treatment, Bioresour. Technol. 238 (2017) 306–312, https://doi.org/10.1016/j.biortech.2017.04.042.
[58] Z. Lian, J. Wang, Selective detection of chloramphenicol based on molecularly imprinted solid-phase extraction in seawater from Jiaozhou Bay, China, Mar. Pollut. Bull. 133 (2018) 750–755, https://doi.org/10.1016/j.marpolbul.2018.06.041.